Comprehensive chemical proteomics analyses reveal that the new TRi-1 and TRi-2 compounds are more specific thioredoxin reductase 1 inhibitors than auranofin

Pierre Sabatier [a], Christian M. Beusch [a], Radosveta Gencheva [b], Qing Cheng [b], Roman Zubarev [a,c,d,**], Elias S.J. Arnér [b,e,*]

[a] *Chemistry I, Department of Medical Biochemistry and Biophysics, Karolinska Institutet, Stockholm, 17177, Sweden*
[b] *Division of Biochemistry, Department of Medical Biochemistry and Biophysics, Karolinska Institutet, Stockholm, 17177, Sweden*
[c] *Department of Pharmacological & Technological Chemistry, I.M. Sechenov First Moscow State Medical University, Moscow, 119146, Russia*
[d] *The National Medical Research Center for Endocrinology, 115478, Moscow, Russia*
[e] *Department of Selenoprotein Research, National Institute of Oncology, 1122, Budapest, Hungary*

ARTICLE INFO

ABSTRACT

Anticancer drugs that target cellular antioxidant systems have recently attracted much attention. Auranofin (AF) is currently evaluated in several clinical trials as an anticancer agent that targets the cytosolic and mitochondrial forms of the selenoprotein thioredoxin reductase, TXNRD1 and TXNRD2. Recently, two novel TXNRD1 inhibitors (TRi-1 and TRi-2) have been developed that showed anticancer efficacy comparable to AF, but with lower mitochondrial toxicity. However, the cellular action mechanisms of these drugs have not yet been thoroughly studied. Here we used several proteomics approaches to determine the effects of AF, TRi-1 and TRi-2 when used at IC50 concentrations with the mouse B16 melanoma and LLC lung adenocarcinoma cells, as these are often used for preclinical mouse models in evaluation of anticancer drugs. The results demonstrate that TRi-1 and TRi-2 are more specific TXNRD1 inhibitors than AF and reveal additional AF-specific effects on the cellular proteome. Interestingly, AF triggered stronger Nrf2-driven antioxidant responses than the other two compounds. Furthermore, AF affected several additional proteins, including GSK3A, GSK3B, MCMBP and EEFSEC, implicating additional effects on glycogen metabolism, cellular differentiation, inflammatory pathways, DNA replication and selenoprotein synthesis processes. Our proteomics data provide a resource for researchers interested in the multidimensional analysis of proteome changes associated with oxidative stress in general, and the effects of TXNRD1 inhibitors and AF protein targets in particular.

1. Introduction

Targeting cellular antioxidant defense systems as a molecular principle for anticancer treatment has been proposed as of late since many cancer cell types produce high levels of reactive oxygen species [1–3] and rely on activation of antioxidant enzymes [4] thus creating potential therapeutic targets [5,6]. The antioxidant defense systems in mammals rely on the thioredoxin and glutathione systems, whereby inhibiting both these systems simultaneously could be a tempting approach for anticancer therapy if it was not lethal also for normal cells [7–9]. Targeting one of the systems has however shown great promises with

compounds like auranofin (AF) inhibiting the selenoprotein TXNRD1 [10], which is an enzyme shown in several studies to be a promising anticancer drug target [11–16]. AF is evaluated in clinical trials for therapy in several forms of cancer such as fallopian tube cancer, ovarian epithelial cancer, primary peritoneal cavity cancer, ovarian serous tumor, ovarian carcinoma, chronic lymphocytic leukemia, small lymphocytic lymphoma, leukemia prolymphocytic, non-small cell lung cancer, adult solid tumor, small cell lung carcinoma, and lung adenocarcinoma (clinicaltrials.gov). AF is an FDA-approved drug (Ridaura®) for use in rheumatoid arthritis; it binds to TXNRD1 as its main target [11,12,17,18]. Several additional targets have however also been

---

described for the drug, including other reductases, glutathione S-transferases, proteasomal deubiquitinases and several phosphatases [11, 19–21]. Therefore, AF is not a TXNRD1-specific inhibitor, and thus it is important to understand what cellular effects of AF depend upon what protein is being targeted. In a drug discovery effort focused on developing more specific TXNRD1 inhibitors, the two compounds named TRi-1 and TRi-2 ("thioredoxin reductase inhibitor −1 and −2") showed promise for inhibiting cancer cell growth in culture as well as in mouse models, while not overtly affecting normal cells or tissues [17]. These compounds have high therapeutic potential with more precisely defined molecular mechanisms of action compared to AF, thus potentially inducing fewer off-target side effects. However, the proteome-wide target landscape of these molecules has not yet been investigated in detail. The purpose of this study is thereby to evaluate the cellular effects of TRi-1 and TRi-2 in comparison to AF using proteomics.

Advances in the chemical proteomics field have enabled several new methods for deconvolution of drug targets and action mechanisms. Functional Identification of Target by Expression Proteomics (FITExP) has recently been used to develop the ProTargetMiner tool and resource [22–24]. The FITExP method uses the peculiarity of cellular proteome responses to toxic compounds during cell death; specifically, the drug target and mechanistic proteins are typically found to be strongly up- or down-regulated. Another method in chemical proteomics is called thermal proteome profiling (TPP), which is a proteome-wide version of the cellular thermal shift assay (CETSA), and is based upon the alteration of thermal stability of proteins upon the binding of drugs or ligands to them. The TPP is an assessment of this property on the whole-proteome level and has been employed to measure drug target engagement in both living cells and in cell lysates [25,26]. Recently, we developed the proteome integral stability alteration (PISA) [27] assay that dramatically increases TPP throughput. The PISA assay utilizes integrated "areas under the curve" of combined samples that have been heated to different degrees, thereby significantly lowering the number of samples that need to be analyzed compared to the TPP method. In order to assess the redox state of cysteine residues in proteins, specific chemical tags enabling such proteomics analyses were developed [28]. In a recent work, we used a combination of these different chemical proteomics methods in order to study the target landscape of AF in a selection of human cancer
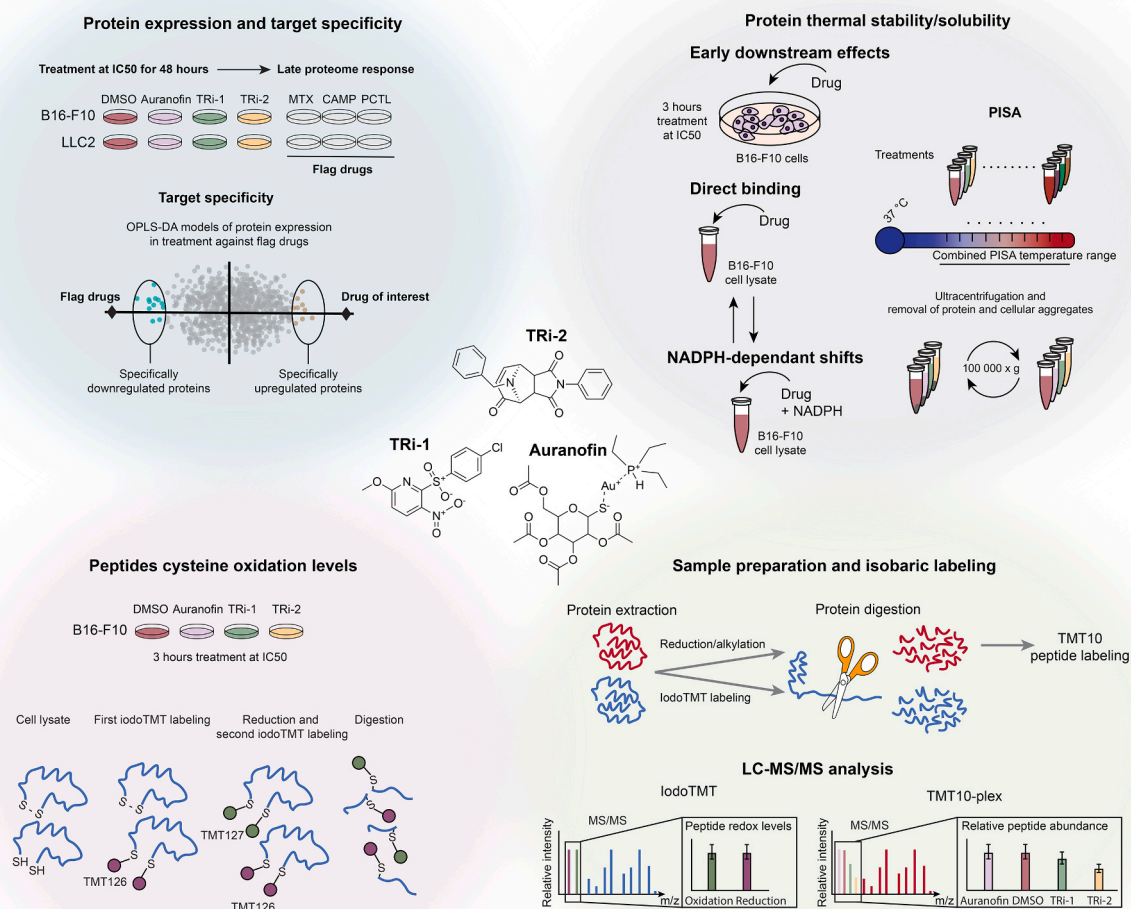
Fig. 1. Workflow. Outline of the experimental strategy using a combination of FITExP, three different type of PISA assays and redox proteomics to deconvolute specific responses upon the use of the three different TXNRD1 inhibitors (structures shown in the middle) using two mouse cancer cell lines.

cell lines, finding that TXNRD1 is one of the main targets of AF together with NFKB2 and CHORDC1 [12]. In the present study we use a similar combination of several proteomics approaches to study the proteome-wide effects of AF in comparisons with those of TRi-1 and TRi-2 (Fig. 1). We used here two mouse cancer cell lines, LLC2 (Lewis Lung Carcinoma) and B16–F10 (melanoma) as these are often used in pre-clinical *in vitro* studies as well as for *in vivo* mouse tumor models in evaluation of anticancer therapeutic efficacy [29–31]. Both the *Txnrd1* gene and the TXNRD1 protein were previously suggested to play key roles in the promotion of tumor development in mice, using both LLC2 [32] and B16 [33], thus underlining the importance of determining the effects of the three inhibitors of this enzyme in these two cell types. The overall conclusion from our results is that TRi-1 and TRi-2 are more specific TXNRD1 inhibitors than AF, and we identify additional targets of the three drugs that should be considered for the understanding of their effects in different mouse cancer models.

2. Materials and methods

2.1. Cell culture

B16–F10 and LLC2 cells were cultured at 37 °C and 5% CO_2 in a humidified Forma Steri-cycle i160 CO_2 incubator (Thermo Fischer Scientific). They were maintained in DMEM (Lonza) supplemented with 10% FBS (Gibco), 2 mM L-glutamine (Lonza) and 150 nM Na_2SeO_3 as additional selenium source to saturate cellular selenoprotein synthesis. Both cell lines were kept for 8 passages at maximum for any of the experiments described below.

2.2. Drug IC50 measurements

B16–F10 and LLC2 were seeded into 96-well plates (Sarstedt) at a density of 3000 cells per well and grown for 24 h. Then, medium was replaced with fresh medium containing the drugs namely AF, TRi-1 and TRi-2. Nine concentrations were tested, including vehicle control (DMSO) or 0.005, 0.05, 0.5, 1, 5, 10, 25 and 50 μM. Four replicate per drug and concentration were used. The treatment was conducted for 48 h, after which, cell viability was measured using CellTiter-Fluor™ following manufacturer's protocol.

2.3. TXNRD1 inhibition assay and determinations of TXNRD1 protein abundances

B16–F10 cells were seeded into 6-well plates (Sarstedt) at a density of 300 000 cells per well. The following day, cells were treated using 4.5 μM, 3 μM and 0.3 μM of auranofin and TRi-2, 30 μM, 20 μM and 2 μM of TRi-1 and vehicle (DMSO) at the same concentration. Cells were collected after 1 h, 3 h and 12 h of treatment using the following procedure. Cells were washed twice with PBS, then 200 μL of lysis buffer (50 mM Tris-HCl, 2 mM EDTA, 0.15 M NaCl, 1% Triton X-100, protease inhibitors (Roche), pH 7.5) was added and cells were scraped, collected into tubes and snap frozen. After three freeze-thaw cycles, cell lysates were centrifuged (13 000 rpm, 15 min), supernatants were collected, and protein concentrations measured using Pierce bicinchoninic acid assay (BCA) protein assay kit (Thermo Fischer Scientific) according to the manufacturer's protocol. To measure TXNRD1 activities, the end-point TXN-dependent insulin reduction assay was used, essentially as described previously [17]. In short, 7.5–9 μg total protein from the cell lysate was incubated with 0.16 mM human insulin (Sigma), 0.33 mM NADPH (Saveen Werner) and 16 μM human TXN (recombinantly produced as previously described [81]) in TE buffer (50 mM Tris-HCl, 2 mM EDTA, pH 7.5) at a total volume of 50 μL and was then incubated at 37 °C. After 0, 15 and 30 min, 10 μL aliquots were taken and combined with 6 M guanidine-HCl and 2.5 mM DTNB in 96-well plates (PerkinElmer), whereupon the absorbance at 412 nm was measured using microplate spectrophotometer (TECAN). Levels of active Txnrd1 were

normalized to DMSO control samples for each treatment timepoint.

Relative protein abundance of TXNRD1 was determined by Western blot. In short, 25 μg total protein from the same cell lysates used above for activity measurements was denatured at 95 °C in LDS sample buffer (Novex Life Technologies) with 10 mM DTT (Sigma) and loaded onto Bolt Plus 4–12% BisTris precast gels (Thermo Fischer Scientific). Electrophoresis was performed at 165 V for 40min, and dry transfer, using iBlot 2 NC transfer stacks (Thermo Fischer Scientific), at 20 V for 7 min. TXNRD1 was detected using an anti-mouse TXNRD1 polyclonal antibody from rabbit serum, kindly provided by G. Merrill, Oregon State University, and GAPDH was detected using rabbit anti-human GAPDH (Santa Cruz Biotechnology, sc25778, LOT D1613). A goat anti-rabbit HRP-IgG secondary antibody (Southern Biotech, 4030-05, LOT A2718-MM00) was used for chemiluminescent signal detection with ECL detection reagent (Cytiva Amersham). Band detection and quantification was performed in Quantity One and Image Lab (BioRad) software. Protein abundance of TXNRD1 was normalized to that of GAPDH with the DMSO control samples for each treatment timepoint set as 100%. For estimations of the amounts of inactive and active TXNRD1 protein in each sample, "inactive TXNRD1" was estimated from the remaining TXNRD1 content according to the Western blot after subtracting the content corresponding to that found in the DMSO control sample, assuming that the DMSO control sample represented 100% active TXNRD1, with the activity of that sample determined above. In samples where the calculated "active TXNRD1 per band intensity" slightly exceeded that determined for the DMSO control, we assumed that no inactive TXNRD1 was present.

2.4. FITExP analysis

B16–F10 and LLC2 were seeded into 6-well plates (Sarstedt) at a density of 100 000 per well and grown for 24 h. Then cells were treated with IC50 concentration of each drug and corresponding concentration of DMSO (Fig. 1). Treatments were conducted in triplicates for each drug and cell lines. After 48 h of treatment, cells were washed two times with PBS, whereupon lysis buffer (1% SDS, 8 M urea, 50 mM Tris pH 8.5) was added on top of the cells. Cells were scraped and collected into tubes and then sonicated using a probe sonicator (Branson) for 45s (3s/3s pulse, 30% amplitude). Protein concentration was measured in each sample using Pierce bicinchoninic acid assay (BCA) protein assay kit (Thermo Fischer Scientific) according to the manufacturer's protocol.

2.5. PISA measurements

B16–F10 cells were grown as described above until around 70% confluence. For the PISA in cell experiment, medium was replaced with fresh medium containing IC50 concentration of AF, TRi-1 and TRi-2 (Fig. 1) with adjusted concentration of DMSO (vehicle) so that DMSO concentration is equal for each drug and the control treatment consisted in the same concentration of DMSO. Cells were then incubated with the drugs for the indicated time, after which cells were washed with PBS and detached using TrypLE Express. The reaction was stopped by adding fresh medium and the cells were pelleted at $340 \times g$ for 2 min. Cell pellets were rinsed two times with PBS and finally the cells were resuspended in 1 mL of PBS supplemented with protease inhibitors (Roche). For the lysate experiments, cells were grown, detached and resuspended in the same way, however, cells were then lysed directly by freezing/thawing cycles in liquid nitrogen. The lysates were cleared by centrifugation at $20\,000 \times g$ for 5 min and lysates were aliquoted for each treatment in triplicates and treated for 30 min with the same concentrations as in the PISA with intact cell experiments. For one of the PISA in lysates experiment, lysates were also supplemented with 1 mM NADPH, added 5 min before addition of compounds. After the treatments for 30 min, 100 μL of the cell suspension or cell lysate were distributed into 10 PCR tubes per replicate (n = 3 for each treatment). Cells were heated in a temperature range from 48 to 59 °C and samples corresponding to each replicate

were combined together. For the PISA in intact cell experiment, cells were lyzed using the same freezing/thawing method as for creating the cell lysates. Finally, for each experiment, samples were transferred to ultracentrifuge tubes, placed into a Ti 42.2 rotor (Beckman-Coulter) and ultracentrifuged at $100\,000 \times g$ for 20 min using an Optima XPN-80 Ultracentrifuge (Beckman-Coulter). 70 μL of the supernatant was collected and the same volume of lysis buffer (8 M urea, 20 mM EPPS pH 8.5) was added and the protein concentration was measured using Pierce bicinchoninic acid assay (BCA) protein assay kit (Thermo Fischer Scientific) according to the manufacturer's protocol.

2.6. Redox proteomics

B16–F10 cells were grown and treated in the same way as for the PISA experiments with intact cells. Cell lysis was performed as in FITExP except that the cells were always kept on ice, until iodoTMT reagents were added to the lysates to label reduced cysteines. IodoTMT reagents were resuspended into methanol and 4.4 mmol/L of a first label were added to the samples and they were incubated at RT for 1 h in the dark. Samples were precipitated using methanol chloroform (see below) and resuspended into HES buffer. Then 1 mM of DTT was added to the samples that were incubated for 1 h at RT to reduce the unlabeled oxidized cysteines. A second iodoTMT label different from the first one was added to the samples at 4.4 mmol/L which were incubated for 1 h at RT in the dark to label the newly reduced cysteines.

2.7. Protein sample preparation for expression proteomics and TMT10 labeling

For all proteomics experiments, 50 μg of proteins were used in sample preparation. Reduction was performed using 5 mM DTT at RT for 1 h followed by alkylation using 15 mM IAA at RT in the dark for 1 h. The reaction was quenched by adding 10 mM DTT. Then methanol/chloroform precipitation was performed as followed: 3 sample volumes of methanol were added, then 1 sample volume of chloroform and 3 volumes of water. Samples were vortexed between each step and then centrifuged at $20\,000 \times g$ for 10 min at 4 °C. The aqueous layer was removed, and the protein pellet was rinsed with one sample volume of methanol, vortexed and centrifuged using the same speed as in the previous step. Finally, all the liquid was removed, and the protein pellet was air-dried.

Air-dried protein pellets were resuspended in 8 M urea, 20 mM EPPS pH 8.5. The samples were diluted once with by adding 20 mM EPPS pH 8.5 (4 M urea) and lysyl endopeptidase digestion was carried out at a 1:100 ratio (LysC/protein, w/w) overnight at RT. The following day, samples were diluted 4 times (1 M urea) with 20 mM EPPS pH 8.5, then tryptic digestion was performed for 6 h at RT using a 1: 100 ratio (Trypsin/protein, w/w). After that, TMT10 labeling were performed during 2 h at RT by adding 0.2 mg of reagent dissolved in dry ACN according to manufacturer's instructions and a final ACN concentration of 20%. The reaction was then quenched by adding triethylamine to a final 0.5% concentration and incubated 15 min at RT. The samples were combined resulting in one pooled sample per replicate containing each temperature. After that, the samples were acidified to pH < 3 using TFA, desalted using Sep Pack (Waters) and vacuum dried overnight using miVac DNA (Genevac).

2.8. High pH reversed-phase peptide fractionation

For the redox proteomics experiments 70 μg of proteins were resuspended into 300 μL of 0.1% TFA and fractionated using Pierce™ High pH Reversed-Phase Peptide Fractionation Kit (Thermo Fischer Scientific) according to manufacturer's protocol, resulting in 8 fractions per sample. Samples were then dried overnight in a Speedvac.

For FITExP and PISA experiments, 150 μg of proteins were resuspended into 20 mM NH₄OH. Then, samples were off-line high-pH

reversed-phase fractionated using an UltimateTM 3000 RSLCnano System (Dionex) equipped with a XBridge Peptide BEH 25 cm column of 2.1 mm internal diameter, packed with 3.5 μm C18 beads having 300 Å pores (Waters). The mobile phase consisted of buffer A (20 mM NH₄OH) and buffer B (100% ACN). The gradient started from 1% B to 23.5% in 42 min, then to 54% B in 9 min, 63% B in 2 min and stayed at 63% B for 5 min and finally back to 1% B and stayed at 1% B for 7 min. This resulted in 96 fractions that were concatenated into 24 fractions and dried overnight using miVac DNA.

2.9. Mass spectrometry analysis

Prior to mass spectrometry analysis, all samples were resuspended in 2% ACN and 0.1% FA at a concentration of 0.2 μg/μL and 1 μg was injected into the respective LC system (Supplementary Table 7). Mass spectra were acquired according to Supplementary Table 8.

2.10. TMT labelling quantification

Protein identification and quantification were performed for all mass spectrometry experiments in the same MaxQuant analysis (version 1.6.2.3) dividing each experiment with the "group" option. MS2 was selected as the quantification mode with TMT10 or iodoTMT as the modification. Acetylation of N-terminal, oxidation of methionine and deamidation of asparagine and glutamine were selected as variable modifications. Carbamidomethylation of the cysteine was selected as fixed modification for TMT10-labelled sample and no modification was selected for iodoTMT-labelled samples. The Andromeda search engine was using the UniProt mouse database excluding protein isoforms (55 228 entries) with the precursor mass tolerance for the first searches and the main search set to 20 and 4.5 ppm, respectively. Trypsin was selected as the enzyme, with up to two missed cleavages allowed; the peptide minimal length was set to seven amino acids. Default parameters were used for the instrument setting. The FDR was set to 0.01 for peptides and proteins. "Match between runs" option was used with a time window of 0.7 min and an alignment time window of 20 min.

2.11. Data normalization and statistical analysis

All data analysis and plots were produced using R version 3.6.1. In all proteomics analysis, individual protein abundances were normalized by the sum of all protein abundances in the corresponding sample. For redox proteomics analysis, individual protein abundances were normalized by the sum of all protein abundances in the corresponding sample and multiplied by the sum of the abundances of the corresponding peptide in each triplicate sample for reduced (TMT126, TMT127 and TMT128) and oxidized (TMT129, TMT130 and TMT131) cysteine separately. Comparison between two sample groups were assessed using two-tailed unpaired t-test unless otherwise specified. Data are presented as mean ± standard error of the mean, unless otherwise stated. P-values lower than 0.05 were considered as statistically significant. r for the corresponding plots were calculated using Pearson correlation. GO pathways enrichment were done using DAVID version 6.8. For pathways enrichment significance, we considered pathways with p-values corrected by Benjamini-Hochberg procedure lower than 0.05. Only proteins identified with two peptides or more and without missing values in any of the samples and replicates were considered for statistical analysis except in redox proteomics experiments.

2.12. Data availability

The mass spectrometry proteomics data have been deposited to ProteomeXchange Consortium (http://proteomecentral.proteomexchange.org) via the PRIDE partner repository with data set identifier PXD028398.

3. Results and discussion

3.1. Determination of auranofin, TRi-1 and TRi-2 cytotoxicity profiles towards LLC2 and B16–F10 cells

We first determined the cytotoxic efficacies of AF, TRi-1 and TRi-2 with the B16–F10 and LLC2 cell lines. This determination was needed for FITExP analyses that require the treatment of several cell lines with IC50 concentrations for 48 h (Fig. 1). AF and TRi-2 exhibited similar efficacies while TRi-1 was less potent (Table 1, Supplementary Fig. 1), in agreement with findings in human cell lines [17]. The slightly higher sensitivity of B16–F10 towards the compounds led us to choose that cell line for the subsequent Txnrd1 inhibition assay, PISA assays and redox proteomics analyses.

3.2. At IC50 concentrations, TRi-1 induces more rapid TXNRD1 inhibition in B16–F10 cells than auranofin or TRi-2

Using the IC50 measurements of AF, TRi-1 and TRi-2 as a standard for efficacy of the drugs (Table 1), we next determined the extent of irreversible TXNRD1 inhibition and relative protein abundance of TXNRD1 in B16–F10 cells upon treatment at earlier time points with either 10% of IC50, IC50 or 150% of IC50 concentrations. We measured both TXNRD1 activity and protein abundance relative to vehicle-treated control samples in cell lysates prepared after 1 h, 3 h and 12 h of treatment. Since the inhibitors are washed away during lysate preparation and cellular proteins become highly diluted in the activity assay, the total activity of TXNRD1 as measured in lysates will reflect that of enzyme being present, which has not been irreversibly inhibited. To our surprise, only TRi-1 showed an early dose-dependent inhibition of TXNRD1 activity, while both AF and TRi-2 required longer incubations with the cells until inhibition of TXNRD1 could be detected. After 1 h of treatment at IC50 and 150% IC50 concentrations, TXNRD1 activity was significantly lowered by TRi-1, while it was increased at 10% of IC50. After 3 h, the TXNRD1 activity was greatly lowered by TRi-1 at 10% of the IC50 concentration and completely abrogated at IC50 and 150% of IC50. Lastly, after 12 h of incubation no significant TXNRD1 activity inhibition was noticeable at any of the tested TRi-1 concentrations, with all samples showing similar activity as the DMSO control. At the 12 h time point, however, both AF and TRi-2 treatment clearly led to less TXNRD1 activity, while these treatments gave little effect on the TXNRD1 activity during the earlier time points (Fig. 2A–C).

We next attempted to estimate the proportion of total TXNRD1 protein in the samples where its activity had been measured. This was important since both active and inactive forms of TXNRD1 can be present, also noting that irreversibly inhibited TXNRD1 may be converted to prooxidant forms of the protein known as SecTRAPs (selenium compromised thioredoxin reductase-derived apoptotic proteins), which are unable to reduce TXN but still capable of redox cycling with NADPH producing reactive oxygen species [34]. Thus, there might be a difference in the triggering of cellular effects when comparing lower amounts of TXNRD1 protein with a lack of TXNRD1 activity due to inhibition of the enzyme. The analyses of TXNRD1 protein abundance clearly demonstrated that non-active TXNRD1 forms could be formed, considering that the samples displaying lower TXNRD1 activities, including the earlier time points of treatment with IC50 or 150% IC50 of TRi-1 that

displayed very low TXNRD1 activities, still contained considerable levels of TXNRD1 protein (Fig. 2D–I, Supplementary Fig. 2). Further analyses of these results revealed that at the early time points only TRi-1 generated large amounts of inactive TXNRD1 protein (Fig. 2I), while inactive forms of TXNRD1 were clearly present after 12 h of treatment with all three compounds (Fig. 2G–I). When assessing the cell shape under these conditions of treatments, we noted that this was clearly affected already after 3 h of treatment with all of the compounds when used at IC50 and 150% of IC50 concentrations (Supplementary Fig. 3A). This suggested that clear effects on cellular integrity were early triggered by all three compounds even if TXNRD1 inhibition could only be detected for TRi-1, where such effects could be early induction of oxidative stress [35–37] or other challenges. We however noted that cell viability, as measured using the CellTiter-Fluor™ reagent, was significantly decreased after 12 h only in the AF treatment at 150% of IC50 and in the TRi-1 treatment at both IC50 and 150% of IC50 concentrations (Supplementary Fig. 3B). The cell death was hence the most rapid for the TRi-1 treatment, while the cell death used for determination of the IC50 values for all three compounds was, as noted above, determined after the longer duration of treatment of 48 h. Taken together, these results could possibly indicate that the TRi-1 cytotoxicity mainly relates to TXNRD1 inhibition and generation of SecTRAPs, while AF and likely also TRi-2 should have additional mechanisms and/or off-target effects that could further contribute to their cytotoxic effects. Previous data have also suggested that both TRi-1 and AF, but not TRi-2, are able to induce formation of SecTRAPs [17]. The fact that AF and TRi-2 showed no detectable inhibition of TXNRD1 at the early time points, but significant inhibition after 12 h of treatment, may also be an indication of different cellular pharmacodynamics of AF and TRi-2 compared to TRi-1, with faster entry and action of the latter compound, and/or may suggest some compensation mechanisms that could maintain TXNRD1 activity during early time points in cells treated with AF or TRi-2. These and other potentially cell type-specific aspects in the actions of these three TXNRD1-targeting compounds should be further investigated, but here we can conclude that TRi-1 is a more efficient TXNRD1 inhibitor than AF and TRi-2 in B16–F10 mouse melanoma cells.

3.3. Auranofin induces wider changes in protein expression and thermal stability profiles than either TRi-1 or TRi-2

Considering the results of the TXNRD1 inhibition assays, we decided to study in more detail the overall effects of AF, TRi-1 and TRi-2 on the cellular proteome, which would be expected to reveal more of their (off-)target landscapes. For this we employed both established and in-house chemical proteomics approaches (Fig. 1). Starting with protein expression abundance measurements, the heatmap and violin plots of protein expression ratios for AF, TRi-1, and TRi-2 treatment at IC50 concentrations as determined after 48 h of treatment showed much broader expression changes in AF treatment compared to the other two drugs, for both the B16–F10 and LLC2 cell lines included in this study (Fig. 3A, Supplementary Table 1). In total the expression levels of 4377 proteins as detected in both cell lines and for all treatments were quantified.

To determine systematic proteome changes during the treatments, we plotted the protein expression fold changes in each cell line against the other (Fig. 3B). The top pathways according to Gene Ontology classifications of "Biological Process", "Molecular Function" and "Cellular Component" that were enriched with proteins showing significantly (p-value <0.05) altered levels in both cell lines and a ≥1.2 or ≤ 0.83 fold change against DMSO control in each cell line are shown in Fig. 3B (full data can be found in Supplementary Table 1). For all three drugs, enzymes involved in oxidoreductase activity and oxidation-reduction process were upregulated, as expected, and most of these proteins were located in the cytoplasm. AF also affected "cell division" and "midbody". Overall, AF activated more pathways than TRi-1 and TRi-2, with the most affected pathways involving "ribosome" and "translation", while both TRi-1 and TRi-2 downregulated proteins from

Table 1
Drug IC50 after 48 h treatment in the corresponding cell lines (n = 4). Growth medium was supplemented with 150 nM selenite and cell viability was assessed using CellTiter-Fluor™. For the IC50 determination curves, see Supplementary Fig. 1.
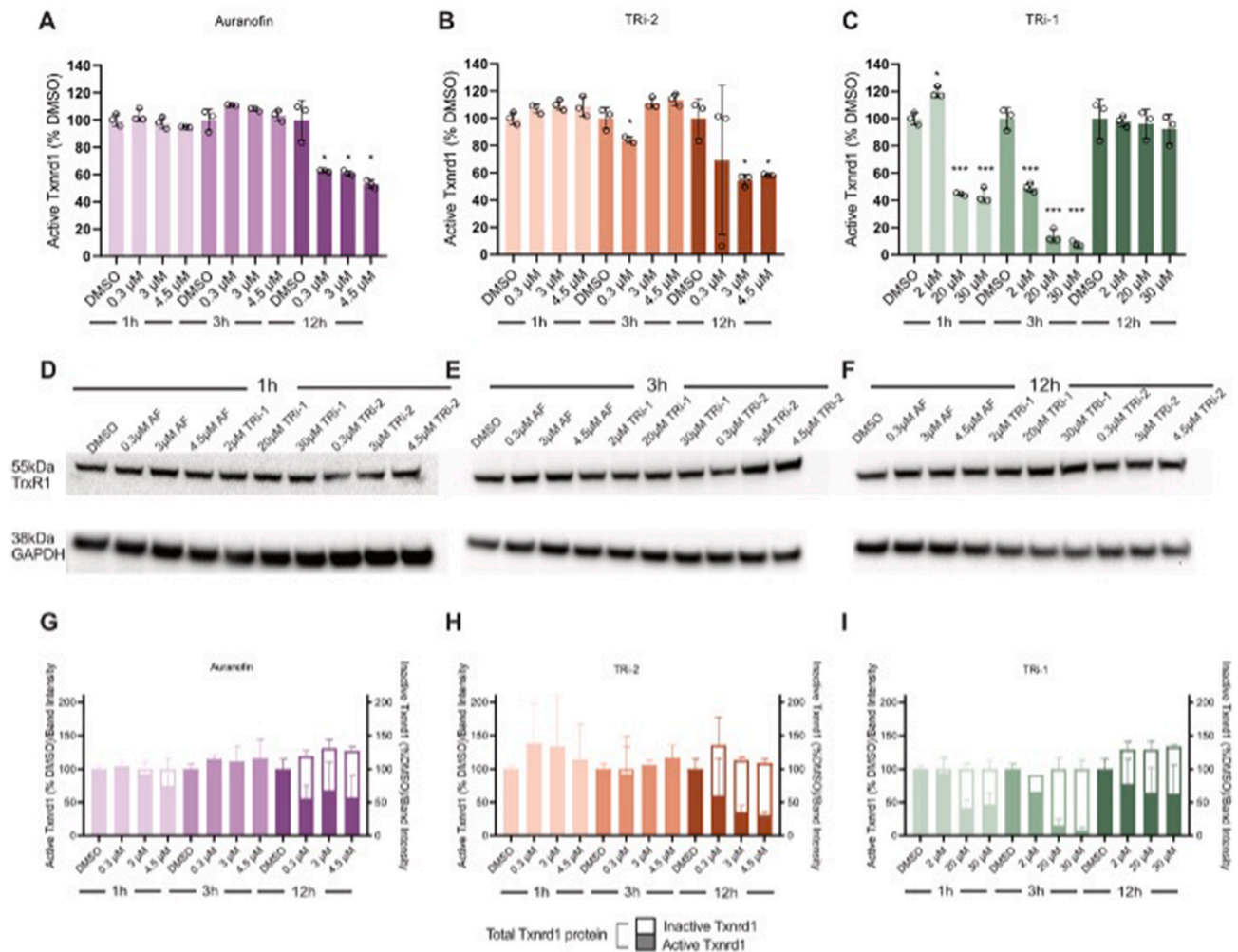
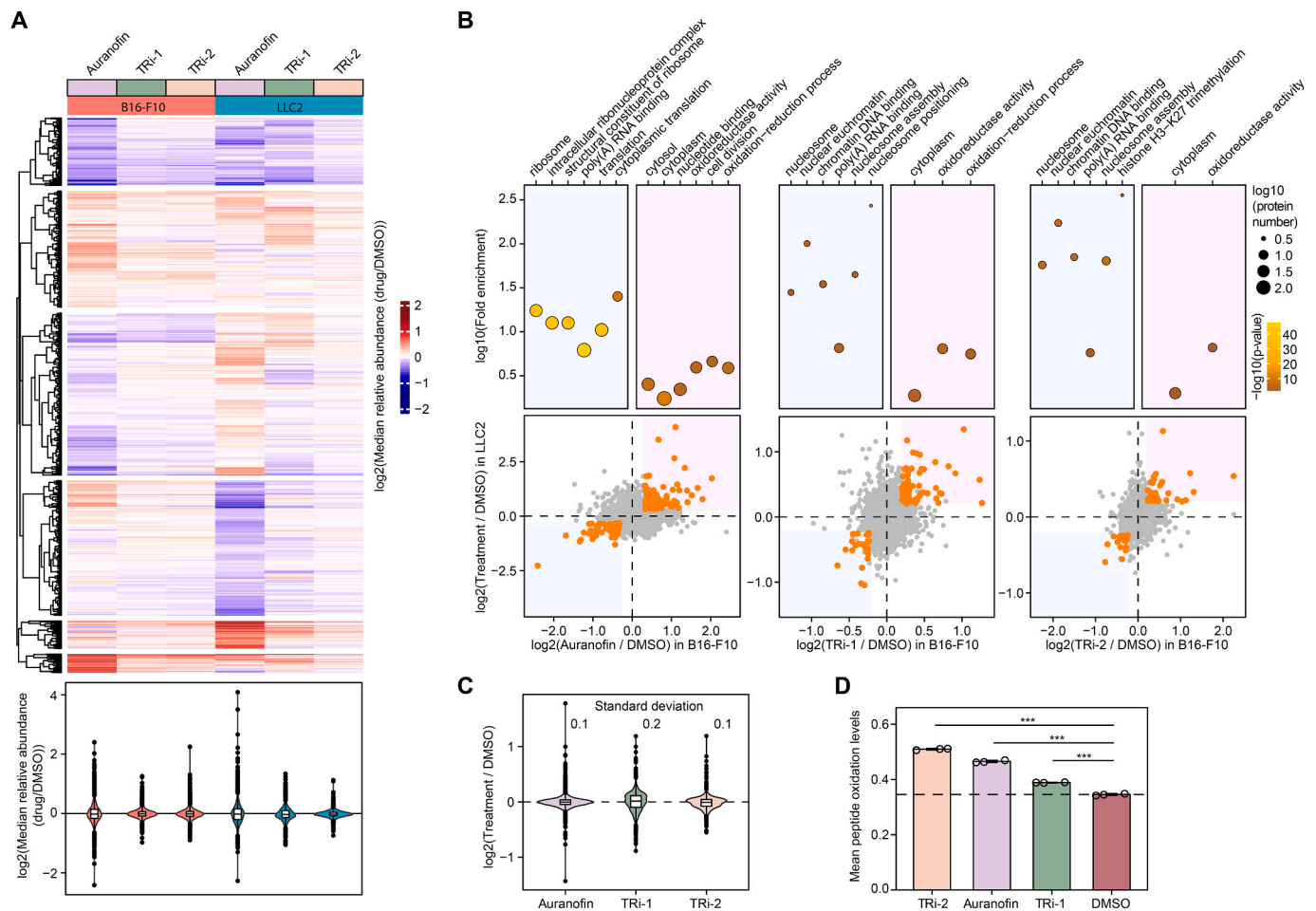|	Auranofin	TRi-1	TRi-2
B16–F10	3 ± 2 µM	20 ± 7.5 µM	3 ± 2 µM
LLC2	7 ± 2.5 µM	25 µM ± 7.5 µM	3.5 ± 2 µM

Fig. 2. Time and dose-dependent inhibition of TXNRD1 relative to total TXNRD1 protein abundance. (A-C) TXNRD1 activity in cell lysates prepared from B16–F10 cells treated with 10% of IC50, IC50 and 150% of IC50 concentrations of each compound (cf. Table 1), as indicated, with (**A**) auranofin treatment at 0.3, 3 and 4.5 μM, (**B**) TRi-2 treatment at 0.3, 3 and 4.5 μM and (**C**) TRi-1 treatment at 2, 20 and 30 μM, with lysates prepared after 1 h, 3 h and 12 h of treatment, as indicated. (**D-F**) Representative Western blot determinations of TXNRD1 and GAPDH protein abundances in the same cell lysates analyzed in (**A-C**) (complete membranes in Supplementary Fig. 2). (**G-I**) Estimations of the amounts of active as well as inactive TXNRD1 protein in the cell lysates, calculated from estimations of the activity measurements relative to the TXNRD1 protein abundances, with calculations normalized for the DMSO controls as described in the Methods section (one biological replicate was excluded from the analysis for 12 h treatment and in (I) two biological replicates for 3 h treatment were excluded, due to lack of sufficient amounts of sample remaining). Error bars represent ± standard deviations from the mean. *P*-values for the activity measurements in (A–C) were calculated using a two-sided paired Student's *t*-test against the respective DMSO, *$p < 0.05$, **$p < 0.05$, ***$p < 0.05$. n = 3.

the "nucleosome" and "nuclear euchromatin" classifications (Supplementary Table 2). Additionally, AF affected "chromosome structure" and "nucleus" (Supplementary Table 2), in line with our previous observations of AF-triggered effects in human cells [12]. In summary, all three compounds triggered an upregulation of redox active enzymes after 48 h of treatment at IC50 in both cell lines. However, AF seemed to differ in its effects from those of TRi-1 and TRi-2 in terms of the magnitude of protein expression alterations, and also moderately in terms of the additionally affected cellular pathways. Effects of AF on ribosome function and translation could perhaps explain the broader expression changes upon AF treatment as secondary downstream events, but additional direct effects on several proteins by AF can of course not be ruled out. AF at higher concentrations can also directly inhibit the proteasome [11,21], contributing to disruption of the protein synthesis verversus protein degradation balance. Thus, the wider global protein expression changes observed upon AF treatment are likely to originate from simultaneous alteration of multiple pathways. The effects on nuclear DNA-related proteins found here with both TRi-1 and TRi-2, but not with AF, are previously non-described effects of these compounds,

which should deserve further studies. Perhaps these effects may relate to targeting of splice forms of TXNRD1 present in the nucleus [38–41], which may possibly affect nuclear DNA organization by mechanisms not yet fully understood.

In subsequent PISA experiments performed in B16–F10 intact cells, cell lysate and cell lysate supplemented with NADPH, the same concentrations of the drugs were used as in the FITExP experiments, with the treatments in this case lasting 3 h for intact cells and 30 min for the lysate experiments. Measuring protein thermal stability/solubility profiles in cells enables assessments of proteins directly targeted by compounds or metabolites, the downstream effects of protein target inhibition, as well as compartment engagement. We have previously demonstrated that protein thermal stability shifts can also be attributed to formation of disulfide bonds or their reduction by reductive enzymes [12,42]. Since TXNRD1 has the capacity to reduce disulfide bonds in substrate proteins, either directly or indirectly through thioredoxin-fold proteins, we expected to be able to study downstream effects of its inhibition with minimal protein expression changes after the shorter 3 h treatment. In the PISA analyses, 4491 proteins were quantified in all of

Fig. 3. Auranofin triggers broader proteome responses than TRi-1 and TRi-2 and all treatments lead to oxidative stress. (A) Heatmap and violin plots of the expression changes upon AF, TRi-1 and TRi-2 treatment at IC50 concentration for 48 h compared to DMSO control in B16–F10 and LLC2 cell lines. (B) Two-dimensional plots of mean protein expression fold change in each treatment for B16–F10 against LLC2 cell lines (bottom) and subsequent GO pathways enrichment analysis using DAVID pathways analysis of proteins that are upregulated or downregulated upon treatment in both cell lines (top). Top 2 pathways at most in GO Biological Process (BP), Molecular Function (MF) and Cellular Component (CC) with p-value corrected by Benjamini-Hochberg procedure <0.05 were considered for enrichment in the GO term analysis. (C) Violin plot of thermal stability changes from PISA assays in B16–F10 cells of each treatment against DMSO, treatments were performed for 3 h. (D) Mean cysteine-containing peptides oxidation levels for each drug and DMSO during 3 h treatment in B16–F10 cells. Error bars represent ± the standard deviations from the mean. *P*-values were calculated using a two-sided paired Student's *t*-test with ***$p < 0.005$. N = 3 for expression and redox proteomics experiments and n = 4 for PISA assay. For raw data and individual protein results, see Supplement.

the treatments and experiments. In evaluations of the results from the PISA in cells, AF was found to yield the largest shifts while TRi-1 led to the highest number of shifts (Fig. 3C, Supplementary Table 1). All the individual 4491 proteins showing changes in the three treatment conditions (intact cells, cell lysates and cell lysates supplemented with NADPH) are listed in Supplementary Table 3 together with their individual fold-changes and p-values between experiments.

Finally, we performed redox proteomics measurements in B16–F10 cells treated for 3 h at IC50. TRi-2 showed the highest mean protein oxidation levels among the 2113 quantified cysteine-containing peptides belonging to 1455 proteins for all of the treatments, then AF, and finally TRi-1 (Fig. 3D, Supplementary Table 1). All compounds increased overall cysteine oxidation in cells compared to DMSO control, as expected. However, contrary to the expression proteomics and PISA assays with intact cells, AF did not exhibit the highest changes in protein oxidation levels.

3.4. TRi-1 and TRi-2 lead to more specific upregulation of TXNRD1 than auranofin

To assess the relative specificity of TRi-1, TRi-2 and AF to their

respective targets, we next performed FITExP analyses by comparing the effects of these compounds with the three "standard" anticancer drugs, methotrexate, paclitaxel and camptothecin, which are known to induce largely non-overlapping death pathways. The OPLS-DA models [24,43] on the data merged from the two cell lines contrasting each test compound against the standard drugs reveal compound-specific responses (Fig. 4A). Notably, NAD(P)H Quinone Dehydrogenase 1 (NQO1) and Glutamate-Cysteine Ligase Catalytic Subunit (GCLC) were specifically upregulated in each treatment by AF, TRi-1 and TRi-2, which would be expected as these two proteins are typical NRF2 targets, and NRF2 activation can often be noted upon TXNRD1 targeting (see further analyses and discussion below). Interestingly, Cytochrome *c* (Cysc) was upregulated for TRi-1 and TRi-2, but downregulated for AF. Cytochrome *c* Oxidase Assembly Factor 7 (Coa7) was also specifically downregulated in AF treatment. Cytochrome *c* can scavenge reactive oxygen species as well as become released from the mitochondria upon oxidative stress [44] and thus initiate apoptosis [45]. The opposite effects on cytochrome *c* levels between the treatments with AF vs. TRi-1 and TRi-2 might perhaps come from different toxicities of these compounds towards the mitochondria, since out of the three compounds, AF is the only one with clearly enhanced mitochondrial toxicity [17]. The
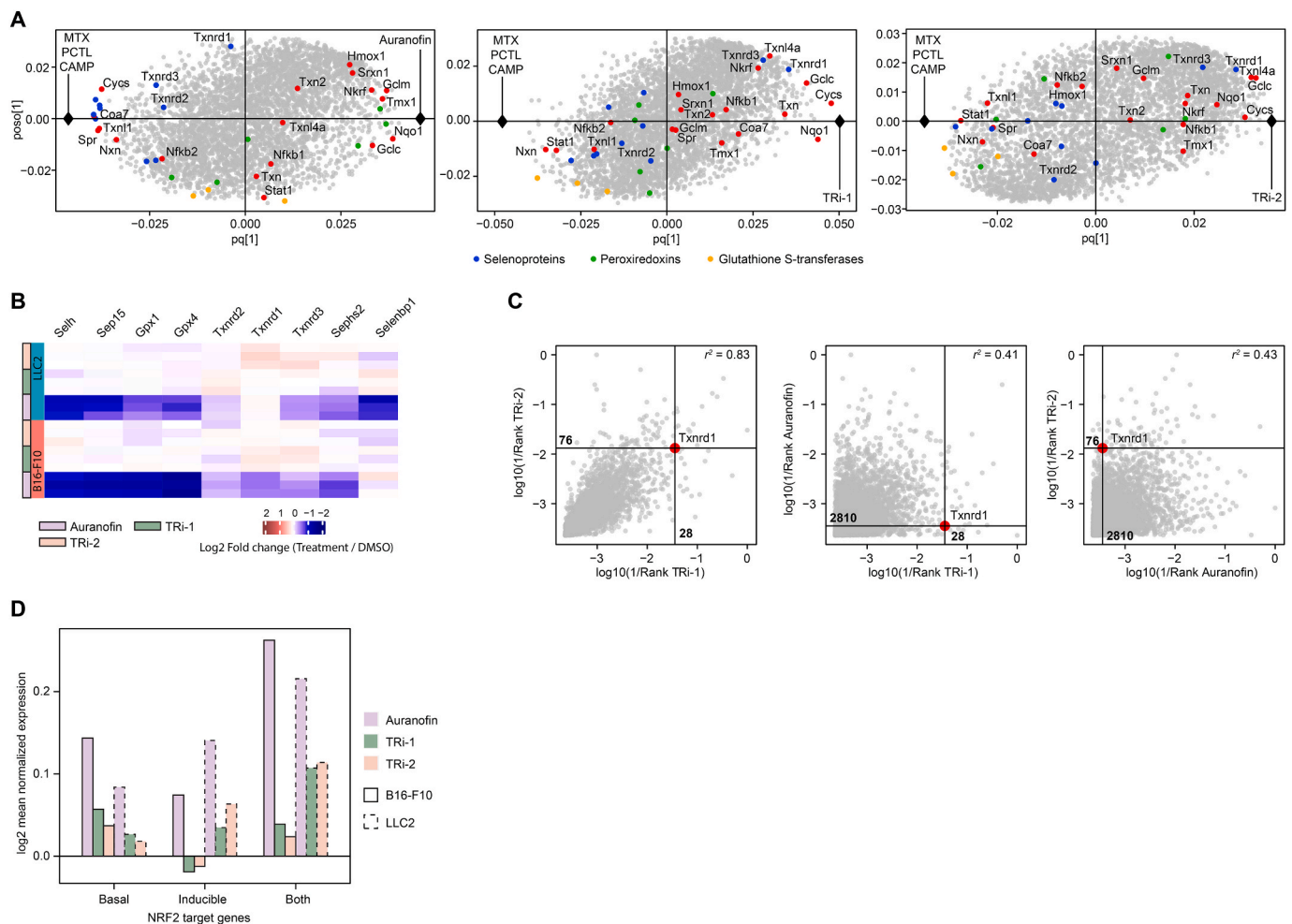
Fig. 4. TRi-1 and TRi-2 specifically upregulate TXNRD1 more than auranofin while only auranofin treatment downregulate selenoproteins and triggers high NRF2-mediated antioxidant response. (A) Analysis of treatment-specific proteome responses using OPLS-DA models to match AF, TRi-1 and TRi-2 protein expression data against Methotrexate, Camptothecin and Paclitaxel as in FITExP [22–24]. Enzymes involved in redox regulation or stress response are highlighted. (B) Two-dimensional plots of the target ranking based on OPLS-DA models output of each treatment against each other. R values were calculated using Pearson correlation. (C) Heatmap of selenoproteins expression fold change of each treatment against DMSO. (D) Mean expression of proteins under control of NRF2 in each treatment (individual protein data are given in Supplementary Table 3). N = 3 for each experiment.

transcription factors nuclear respiratory factor 1 (NRF-1) and cAMP-response element-binding protein (CREB) have been shown to mediate upregulation of *Cycs* transcription [46] but the possible mechanisms for *Cycs* activation by TRi-1 and TRi-2 need yet to be validated. Lastly, AF treatment triggered specific downregulation of many selenoproteins in the FITExP analysis, in line with previous observations showing that AF inhibits selenoprotein synthesis [47] (Fig. 4A). We indeed detected strong downregulation of most selenoproteins upon treatment with AF, in terms of abundance levels, while interestingly no significant variations in selenoprotein levels were observed for TRi-1 and TRi-2 (Fig. 4B).

When the rank of TXNRD1 among the proteins according to their first OPLS-DA component was compared for the different treatments, TRi-1 and TRi-2 (28th and 76th rank, respectively) were clearly superior to that of AF (2810th) (Fig. 4C). In addition, TRi-1 and TRi-2 also showed the best correlation between their ranks, with a r^2 of 0.83, while their correlation with AF was 0.41 and 0.43, respectively (Fig. 4C).

Finally, we used OPLS-DA models contrasting the effects of each drug (AF, TRi-1 and TRi-2) against the other two, in order to further highlight their possible differences in specificity towards TXNRD1 within the proteome landscape. We furthermore ranked all detected proteins according to the coordinates of their first component in decreasing order. TXNRD1 was thereby ranked at positions 521, 869 and 4051 in TRi-2,

TRi-1 and AF treatments, respectively (Supplementary Table 4). Thus, TRi-2 showed more specific upregulation of TXNRD1 in this analysis, followed by TRi-1 and AF. Selenoproteins were specifically downregulated, with SEP15 and SELH ranking last and second to last in AF compared to TRi-1 and TRi-2, thus confirming the trend of the AF-specific effects on general selenoprotein expression (Supplementary Table 4). Target rankings in OPLS-DA models thereby further strengthen the notion that TRi-1 and TRi-2 are more specific TXNRD1 inhibitors than AF, and that only AF triggers specific downregulation of selenoproteins.

3.5. Auranofin triggers more potent NRF2 activation than TRi-1 and TRi-2

Since many proteins specifically upregulated in AF treatment are known to be induced by activation of the NRF2 transcription factor [48, 49], such as NQO1, HMOX1, GCLM and GCLC (Fig. 4A), we analyzed the average expression of proteins with a promoter that is under control of NRF2 at the basal level, only when induced, and in both cases [50] (Supplementary Table 5). AF showed the highest mean protein expression changes in both cell lines for the corresponding basal and inducible NRF2-dependent genes, as well as for NRF2-target genes that fit in both categories (Fig. 4D). TRi-1 and TRi-2 gave moderate to no changes in

these protein levels, however with slightly higher changes in the LLC2 cell line for the NRF2-inducible proteins, and in both cell lines for basal as well as inducible genes (Fig. 4D). AF is known to also target mitochondrial TXNRD2, creating redox stress in the mitochondria [51]. NRF2 however protects also mitochondria from oxidative stress by increasing the expression of antioxidant enzymes [52,53]. AF may also inhibit proteins from the glutathione system including, at least at high concentrations, glutathione peroxidase 1 (GPX1) [17] and, as shown herein, AF lowers the levels of many selenoproteins. Since many selenoproteins have antioxidant function, it may thus be that the wider effects of AF trigger a rather strong oxidative stress in cells, in spite of its strong effects with NRF2 activation. It should however be noted that the overall outcome in terms of the extent of triggered oxidative stress will be context dependent, and the protective functions of NRF2 activation can in certain cell types and conditions be the major effect of AF treatment [48,54,55]. Even though our redox proteomics data show that AF induces high oxidation levels in proteins, thus indicative of higher oxidative stress, TRi-2 induced even higher oxidation levels in the cellular proteins. AF triggered NRF2-mediated responses, while the more specific TXNRD1 inhibitors were interestingly found here to only have partial responses, at best, with regards to NRF2 activation. Taken together, these observations suggest that inhibition of TXNRD1 alone is not sufficient to trigger a high NRF2 response, although many inhibitors of TXNRD1 as well as genetic knockout of the enzyme have been found to activate NRF2 [56]. The functional links between TXNRD1 targeting and NRF2 activation clearly need to be further studied.

3.6. PISA analyses reveal the target landscape of each treatment and suggest higher specificity of TRi-1

We know from previous work [12] that TXNRD1 shows only a subtle thermal stability shift in TPP in cells and no shift in cell lysates when inhibited by a targeting compound, which likely is due to its highly flexible C-terminal tail encompassing the active site selenocysteine residue that is typically the specific target of compounds inhibiting the enzyme [57]. Consequently, we performed PISA analyses to study the target landscape of each compound, bearing in mind that TXNRD1 will most likely not be highlighted in such analyses. As additional experimental control, we performed the PISA assay protocol using B16–F10 lysate supplemented with NADPH. We added NAPDH to the cell lysate in both treated and control samples in one of the PISA analyses, in order to keep the activity of NADPH-dependent enzymes, allow for NADPH-dependent reduction of TXNRD1 with exposure of its Sec residue, and particularly to allow for possible pro-oxidant NADPH oxidase activities of inhibited TXNRD1 turned into SecTRAPs [34,58].

As expected, we detected no significant difference in the direct TXNRD1 thermal stability/solubility for the three compounds in PISA analyses in cells, lysate or lysate supplemented with NADPH (Supplementary Table 4). However, the combined analyses highlighted other known targets of AF, as well as previously unknown potential targets of AF, TRi-1 and TRi-2 (Fig. 5A, B and C). Notably, we detected stabilization of CCS, GLOD4, RRM1 and GAPBP1 upon AF treatment; these proteins have also been highlighted in the TPP analysis presented in our previous work [12]. For the sake of presentation, in Fig. 5 we have only annotated a few of the proteins showing altered stability/solubility in the volcano plots but the exhaustive list of the PISA hits for the three compounds, as well as the mean fold change against DMSO control and p-value for all proteins quantified in the experiments, can be explored in Supplementary Table 3.

To combine the results of the three PISA assays and determine potential target hits, we tailored our analyses for three different experimental setups, with the different versions of PISA that we have used being complementary but also harboring fundamental differences. In experiments using intact cells, direct inhibition of a protein target can often lead to downstream effects leading to potential false positives (with regards to identification of possible direct targets). Any drug can

also be metabolized in cells, with the metabolites having additional effects. With PISA in cell lysates, such effects are attenuated due to the dilution of proteins and metabolites, and in that case there are also no cellular compartments or metabolic effects that can affect the result. However, using cell lysates increreases the risk of false positive hits due to the lack of organellar compartmentalization. Finally, the use of cell lysate supplemented with NADPH allows for support of redox active enzymes using NADPH, such as TXNRD1, thus leading to a potential detection of additional NADPH-dependent and TXNRD1-or SecTRAP-activity related target effects. All these factors can potentially trigger either false positives or false negatives, which needs to be considered. Thus, we added an additional fold change cutoff and identified as target hits only proteins shifting significantly (p-value <0.05 and log2 fold change $\geq$ abs(log2(1.2))) in at least two PISA experiments (either in cells, lysate, or lysate supplemented with NADPH) for each of the drugs (Fig. 5C).

AF gave 38 target hits including GPX1, a selenoprotein and a known direct target of the AF at least when used at high concentrations [17]. GPX1 showed significantly altered thermal stability in all PISA assays with AF with p-value < 0.05, however in the experiment with intact cells the fold change was lower than in lysate and lysate with addition of NADPH; this difference was likely due to the influence of the cellular environment. Thus, GPX1 did not pass our criteria for the PISA assay in the experiments with cells but is still highlighted as a target hit using our cut-off approach. Conversely, we detected stabilization of HMOX1 in all PISA assay performed in cells, but it was not highlighted as significant in any of the lysate experiments for any of the drugs (either with or without NADPH) and thus HMOX1 was not considered as a target hit. Its stabilization in cells is probably due to downstream effects of TXNRD1 inhibition in a cellular context, as also seen in the FITExP results shown above. It has also previously been shown that HMOX1 expression is upregulated by the loss of TXNRD1 activity [59]. These observations collectively suggest that our analyses offer sufficient flexibility to include potential false negative hits while keeping stringency to lower the number of false positive hits, and the results can yield additional insights into the effects of TXNRD1 targeting when considering the specific results of each experimental setup in the PISA analyses.

Other relevant target hits of AF included GSK3A, GSK3B, MCMBP and EEFSEC (Supplementary Table 3). Both GSK3 proteins affect a multitude of cellular pathways, including glycogen synthesis, WNT signaling and inflammation [60]: e.g., GSK3 inhibitors have anti-inflammatory properties [61]. Thus, AF anti-inflammatory properties might originate at least in part from the inhibition of GSK3A and GSK3B. MCMBP is stabilized upon AF treatment in the three PISA assays (Supplementary Fig. 4A). On the contrary, most members of the MCM complex family (Mcm2-7) are destabilized. MCMBP is important for DNA replication initiation and elongation, and acts as a chaperon for Mcm2-7 [62] that can dissociate the MCM complex, likely by destabilization of the individual subunits [63]. Previous studies have shown that proteins in complex have higher thermal stability than their dissociated counterpart [64]. Recently, Boullosa et al. [65] have shown that AF increases DNA damage in cancer cells. Lower activity of MCMBP leads to genome instability and increased DNA damage [62,66]. Our data could thereby suggest that destabilization of the MCM complex members stems from AF binding to MCMBP, resulting in increased DNA damage over time. Finally, one of the target hits of AF was EEFSEC (Fig. 5B and C, Supplementary Table 3). EEFSEC is the translation factor responsible for incorporation of selenocysteines into selenoproteins [67]. Selenium depletion leads to global decrease in expression of selenoproteins [68–70] while selenium supplementation prior to AF treatment at low doses was shown to attenuate cell lethality [71]. EEFSEC was specifically downregulated with a ranking of 4126 out of 4377 proteins in OPLS-DA of AF against TRi-1 and TRi-2 (Supplementary Table 4). Thus, inhibition of EEFSEC could explain the downregulation of selenoproteins after 48 h of treatment through lower efficiency in the incorporation of selenocysteines into selenoproteins as

Fig. 5. PISA highlights the broader target landscapes of auranofin and TRi-2 compared to that of TRi-1. (**A**) PISA assay in cells for AF, TRi-1 and TRi-2 against DMSO treatment. (**B**) PISA assay in cell lysates for AF, TRi-1 and TRi-2 against DMSO treatment. (**C**) PISA assay in cell lysates supplemented with NAPDH for AF, TRi-1 and TRi-2 against DMSO treatment. (**D**) Venn diagrams of target hits having p-value <0.05 and log2 FC ≥abs(log2(1.2)) in at least one PISA experiment. N = 4 for each experiment; *p*-value were calculated using a two-sided paired Student's *t*-test, significant proteins were the most outliers with p-value <0.05.

part of the AF cytotoxic effect.

Among the 15 TRi-1 target hits, only OXNAD1 and PRDX3 are clearly linked to redox mechanisms. TRi-2 on the contrary had 37 target hits, including aldo-keto reductase family 1, member B8 (AKR1B8) as a protein that passed the cutoff in all PISA experiments (Fig. 5D, Supplementary Fig. 4B). Two other members of the aldo-keto reductase (AKR) family 1, AKR1B7 and AKR1B10 were also significantly shifting in PISA assays in both intact cells and lysate (Fig. 5D, Supplementary Fig. 4B). AKR1B1 showed a slight shift in cell experiments but only passed our selection criteria in the PISA assay in lysate (Supplementary Fig. 4B). These enzymes are NADPH-dependent oxidoreductases involved in various cellular function and have been implicated in several diseases and in cancer onset, as well as in resistance to therapy [72,73]. Development of AKR inhibitors is underway and data highlight the utility of such compounds in diabetes, inflammation, in specific types of cancer and even in heart valve calcification [74–79]. Our data thus suggest that TRi-2 is an AKR inhibitor, in addition to being a TXNRD1 inhibitor, possibly thereby increasing the potential and versatility of the compound for usage in targeted therapies for several diseases. Since inhibition of AKRs has shown anti-cancer effect, this could also help to explain the higher potency of TRi-2 in cancer cells, in terms of efficacious concentrations, when compared to TRi-1.

Proteins that were present as target hits with several of the compounds include peroxisome assembly factor 2 (PEX6) which showed high stabilization in all treatments. However, the repeatability of this result among the replicates was low, and it did not have a significant p-value in TRi-2 and lysate experiments in all drugs. Altered thermal stability of PEX6 could come from an abnormal melting behavior of the protein and the lack of reproducibility as it is a membrane protein and warrants caution in whether these drugs really bind to it and modulate its activity. Splicing factor 45 (SPF45) was significantly shifting in both PISA assays in lysate and lysate + NADPH for both AF and TRi-2. Interestingly, histone acetyltransferase 1 (HAT1) was shifting in both PISA assays in lysate and lysate + NADPH for TRi-1 and TRi-2 and both drugs show downregulation of nucleosome, nucleosome assembly and nuclear euchromatin after 48 h of treatment. However, since HAT1 was not shifting in PISA assay in lysate, it could be a downstream effect of the treatments.

Overall, our PISA analyses showed that AF had the highest number of target hits (38) followed by TRi-2 (37) and TRi-1 (15), again showing how AF has the broadest target landscape of these three compounds. It should, finally, be noted that TRi-1 led to significantly more shifts in

lysate when NADPH was added (cf. Fig. 4B and C), which indeed could potentially be explained by the induction of SecTRAP activity in TXNRD1 inhibited by TRi-1 [17], which should lead to oxidation of downstream targets in the presence of NADPH, while direct TRi-1 target proteins are very few apart from TXNRD1. This result also corroborates our findings of a large proportion of inactive TXNRD1 protein formed in cells, likely being SecTRAPs, following TRi-1 treatment (Fig. 2I).

3.7. Redox proteomics highlights early effects of TXNRD1 inhibition and oxidative stress on the translation machinery and on cell metabolism

To compare the effects of each treatment on cysteine oxidation patterns in proteins of certain cellular pathways, we next performed pathway analyses of the proteins that had peptides showing significant increases or decreases in oxidation levels in B16–F10 cells treated with AF, TRi-1 or TRi-2 as compared to DMSO control (Fig. 6). Surprisingly, most of these pathways were common between the three drugs (Supplementary Table 6). Additionally, the correlation of peptide oxidation percentages was rather similar between TRi-2 and AF, TRi-1 and AF and TRi-1 and TRi-2, with r of 0.57, 0.53 and 0.51, respectively. However, the magnitudes of the changes in oxidation levels after treatment with TRi-1 were much lower than with AF or TRi-2. These findings demonstrate that the general cysteine-containing peptides targets of oxidation are similar between the tested compounds, and that such oxidation affects similar pathways, which were particularly related to translation and energy metabolism. Since only TRi-1 inhibits TXNRD1 activity after 3 h of treatment at IC50, the higher cysteine oxidation triggered by AF and TRi-2 could likely originate, at least in part, from off-target effects beyond TXNRD1 inhibition and could likely involve mitochondrial targeting. Both AF and TRi-2 had multiple oxido-reductases as target hits in the PISA analyses, suggesting that inhibiting these additional proteins may have contributed to an increased oxidative stress in the cells. Further, this finding may also suggest that interactions of AF and TRi-2 with these additional oxidoreductases could indirectly trigger early compensation mechanisms, such as more potent NRF2 activation upon AF treatment in B16–F10.

The GO biological processes that were the most enriched were "aerobic respiration", "translation", "protein folding", "cell-cell adhesion", "cellular response to inteleukin-4 "and "glucose metabolic process" (Fig. 6). All of these pathway perturbations were represented by several protein aberations in the different treatments, apart from "cellular response to interleukin-4" that was represented by only a few
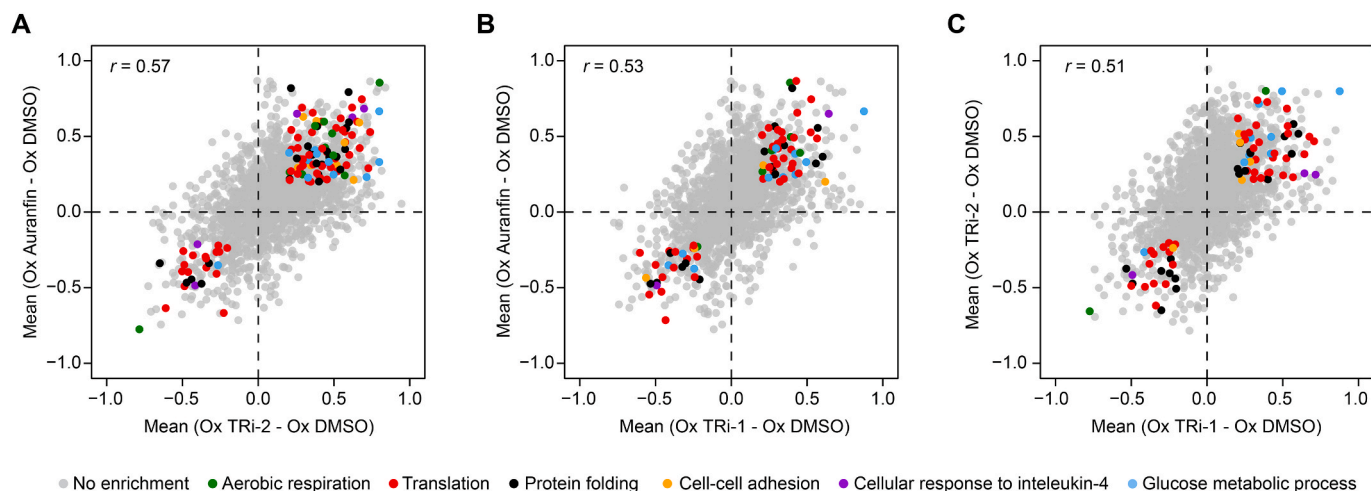
Fig. 6. Redox proteomics highlights similar effects of the treatments on cysteine oxidation. (**A**), (**B**) and (**C**) Two-dimensional plot of cysteine-containing peptides oxidation level compared to DMSO control of AF, TRi-1 and TRi-2 treatments against each other in B16–F10 cells. GO enrichment analysis using DAVID pathways analysis was performed and top significant pathways according to their Benjamini-Hochberg corrected p-value were selected (p < 0.05) and highlighted in the plots. The mean oxidation level difference for each treatment against DMSO was plotted. The r value was calculated using Pearson correlation. N = 3 for each treatment.

proteins. Overall, the AF, TRi-1 and TRi-2 compounds affected similar proteins in terms of these analyses of increased cysteine oxidation on a proteome level.

4. Conclusions

We have here studied the effects on the cellular proteome of three anticancer drug lead compounds that all target TXNRD1. Of these compounds, AF is a known pan-TXNRD inhibitor with several other off-targets, while TRi-1 and TRi-2 were recently selected as top hits from directed TXNRD1 inhibition screenings [17] and have hitherto been considered to be more specific TXNRD1 inhibitors than AF. Our results confirm that TRi-1 and TRi-2 are indeed more specific inhibitors of TXNRD1 than AF, with TRi-1 seemingly having the least off-targets out of the three compounds. In addition, only TRi-1 seems to rely heavily on early TXNRD1 inhibition for its anticancer effects, at least in the two mouse cell lines analyzed here, while auranofin and TRi-2 showed later effects on TXNRD1 activities suggesting that for these two compounds other protein targets could be more likely to contribute to cell death along with the TXNRD1 inhibition.

Capitalizing on the ability of the three drugs to inhibit TXNRD1, we studied target-specific, as well as off-target features of each treatment. AF was, surprisingly, the only compound of the three triggering a strong NRF2 response at IC50 for 48 h treatments, suggesting that TXNRD1 targeting as such is perhaps not sufficient to trigger a strong NRF2 response. Since previous studies have suggested that this would be the case [56], this is an intriguing finding that needs to be further scrutinized.

The PISA analyses highlighted EEFSEC, GSK3A and GSK3B and MCMBP as target hits of AF, which would explain at least in part the downregulation of selenoproteins, metabolic effects, anti-inflammatory effects and DNA damages that are typically and specifically observed upon AF treatment. These processes have been previously described in AF treatment, but their molecular foundations have remained elusive [47,65]. TRi-2 target hits were here found to also include four members of the aldo-keto reductase family, thus potentially increasing the therapeutic potential of this compound in therapies targeting these enzymes and in other diseases than cancer [80]. Target hits for TRi-1, which may be downstream oxidized proteins following formation of SecTRAPs, included OXNAD1 and PRDX3, two redox-related enzymes. Taken together, our data as presented here can be used as a foundation to investigate specific effects of TXNRD1 inhibition, as well as to better understand AF-induced effects on the cellular proteome that may not necessarily be due to TXNRD1 targeting. With our model system being two mouse-derived cancer cells lines, the results should also help to further understand the *in vivo* effects in mouse tumor models used for the evaluation of TXNRD1 inhibitors as anticancer drug leads.

Considering our experimental strategy in general, we have demonstrated here that a combination of chemical proteomics approaches is not only useful in drug target deconvolution, but also helpful for studying the target landscape of drugs in general. The results of this study yielded much broader information on the mechanisms of action of AF, TRi-1 and TRi-2, rather than merely confirming that these three compounds bind to and inhibit TXNRD1 [11,12,17]. Furthermore, we used a combination of chemical proteomics methods and a combination of drugs having one target in common, to deconvolute and distinguish effects that are solely due to inhibition of the known target from those being individual drug-specific effects. Thus, the experimental strategy used herein can serve as a blueprint for future chemical proteomics studies aimed at elucidating drug mechanisms of action.

Author contributions

E.S.J.A. and R.Z. conceived the study, directed experiments, and wrote the manuscript. P.S. performed the proteomics experiments, analyzed the data, and wrote the manuscript. C.B. helped with proteomics experiment and data analysis. R.G. performed the TXNRD1 inhibition and abundance assays and analyzed the data. Q.C. helped with TXNRD1 inhibition experiments and data analysis and produced recombinant TXN. All authors helped finalizing the manuscript.

Declaration of competing interest

E.S.J.A. is co-inventor and co-owner of patents on the TRi-1 and TRi-2 compounds that have been licensed to a company developing them towards clinical applications.

Appendix A. Supplementary data

Supplementary data to this article can be found online at https://doi.org/10.1016/j.redox.2021.102184.

References

[1] T.P. Szatrowski, C.F. Nathan, Production of large amounts of hydrogen peroxide by human tumor cells, Cancer Res. 51 (1991) 794–798.

[2] S. Kawanishi, Y. Hiraku, S. Pinlaor, N. Ma, Oxidative and nitrative DNA damage in animals and patients with inflammatory diseases in relation to inflammation-related carcinogenesis, Biol. Chem. (2006), https://doi.org/10.1515/BC.2006.049.

[3] S. Toyokuni, K. Okamoto, J. Yodoi, H. Hiai, Persistent oxidative stress in cancer, FEBS Lett. (1995), https://doi.org/10.1016/0014–5793(94)01368-B.

[4] B. Marengo, et al., Redox homeostasis and cellular antioxidant systems: crucial players in cancer growth and therapy, Oxid. Med. Cell. Longev. (2016), https://doi.org/10.1155/2016/6235641.

[5] D. Trachootham, J. Alexandre, P. Huang, Targeting cancer cells by ROS-mediated mechanisms: a radical therapeutic approach? Nat. Rev. Drug Discov. (2009) https://doi.org/10.1038/nrd2803.

[6] J. Watson, Oxidants, antioxidants and the current incurability of metastatic cancers, Open Biol. (2013), https://doi.org/10.1098/rsob.120144.

[7] S. Eriksson, J.R. Prigge, E.A. Talago, E.S.J. Arnér, E.E. Schmidt, Dietary methionine can sustain cytosolic redox homeostasis in the mouse liver, Nat. Commun. (2015), https://doi.org/10.1038/ncomms7479.

[8] J.R. Prigge, et al., Hepatocyte DNA replication in growing liver requires either glutathione or a single allele of txnrd1, Free Radic. Biol. Med. (2012), https://doi.org/10.1016/j.freeradbiomed.2011.11.025.

[9] P.K. Mandal, et al., Loss of thioredoxin reductase 1 renders tumors highly susceptible to pharmacologic glutathione deprivation, Cancer Res. (2010), https://doi.org/10.1158/0008–5472.CAN-10-1509.

[10] S. Gromer, L.D. Arscott, C.H. Williams, R.H. Schirmer, K. Becker, Human placenta thioredoxin reductase: isolation of the selenoenzyme, steady state kinetics, and inhibition by therapeutic gold compounds, J. Biol. Chem. 273 (1998) 20096–20101.

[11] X. Zhang, et al., Repurposing of auranofin: thioredoxin reductase remains a primary target of the drug, Biochimie (2019), https://doi.org/10.1016/j.biochi.2019.03.015.

[12] A.A. Saei, et al., Comprehensive chemical proteomics for target deconvolution of the redox active drug auranofin, Redox Biol. (2020), https://doi.org/10.1016/j.redox.2020.101491.

[13] R. Gencheva, E.S.J. Arnér, Thioredoxin reductase inhibition for cancer therapy, Annu. Rev. Pharmacol. Toxicol. 62 (2022).

[14] E. Chupakhin, M. Krasavin, Thioredoxin reductase inhibitors: updated patent review (2017-present), Expert Opin. Ther. Pat. 31 (2021) 745–758.

[15] H. Ghareeb, N. Metanis, The thioredoxin system: a promising target for cancer drug development, Chem. Eur J. 26 (2020) 10175–10184.

[16] F. Mohammadi, A. Soltani, A. Ghahremanloo, H. Javid, S.I. Hashemy, The thioredoxin system and cancer therapy: a review, Cancer Chemother. Pharmacol. 84 (2019) 925–935.

[17] W.C. Stafford, et al., Irreversible inhibition of cytosolic thioredoxin reductase 1 as a mechanistic basis for anticancer therapy, Sci. Transl. Med. (2018), https://doi.org/10.1126/scitranslmed.aaf7444.

[18] C. Marzano, et al., Inhibition of thioredoxin reductase by auranofin induces apoptosis in cisplatin-resistant human ovarian cancer cells, Free Radic. Biol. Med. (2007), https://doi.org/10.1016/j.freeradbiomed.2006.12.021.

[19] S. Tian, F.M. Siu, C.N. Lok, Y.M.E. Fung, C.M. Che, Anticancer auranofin engages 3-hydroxy-3-methylglutaryl-coenzyme A reductase (HMGCR) as a target, Metallomics (2019), https://doi.org/10.1039/c9mt00185a.

[20] A. De Luca, C.G. Hartinger, P.J. Dyson, M. Lo Bello, A. Casini, A new target for gold (I) compounds: glutathione-S-transferase inhibition by auranofin, J. Inorg. Biochem. (2013), https://doi.org/10.1016/j.jinorgbio.2012.08.006.

[21] N. Liu, et al., Clinically used antirheumatic agent auranofin is a proteasomal deubiquitinase inhibitor and inhibits tumor growth, Oncotarget (2014), https://doi.org/10.18632/oncotarget.2113.

[22] A. Chernobrovkin, C. Marin-Vicente, N. Visa, R.A. Zubarev, Functional Identification of Target by Expression Proteomics (FITExP) reveals protein targets and highlights mechanisms of action of small molecule drugs, Sci. Rep. 5 (2015) 11176.

[23] M. Gaetani, R.A. Zubarev, Functional identification of target by expression proteomics (FITExP), in: Mass Spectr. Based Chem. Proteom., 2019, https://doi.org/10.1002/9781118970195.ch10.

[24] A.A. Saei, et al., ProTargetMiner as a proteome signature library of anticancer molecules for functional discovery, Nat. Commun. 10 (2019) 5715.

[25] R. Jafari, et al., The cellular thermal shift assay for evaluating drug target interactions in cells, Nat. Protoc. (2014), https://doi.org/10.1038/nprot.2014.138.

[26] M.M. Savitski, et al., Tracking cancer drugs in living cells by thermal profiling of the proteome, Science 346 (2014) 1255784.

[27] M. Gaetani, et al., Proteome integral solubility alteration: a high-throughput proteomics assay for target deconvolution, J. Proteome Res. 18 (2019) 4027–4037.

[28] Z. Qu, et al., Proteomic quantification and site-mapping of S -nitrosylated proteins using isobaric iodoTMT reagents, J. Proteome Res. (2014), https://doi.org/10.1021/pr401179v.

[29] C.T. Winkelmann, S.D. Figueroa, T.L. Rold, W.A. Volkert, T.J. Hoffman, Microimaging characterization of a B16-F10 melanoma metastasis mouse model, Mol. Imag. (2006), https://doi.org/10.2310/7290.2006.00011.

[30] P. D`Arcy, et al., Inhibition of proteasome deubiquitinating activity as a new cancer therapy, Nat. Med. (2011), https://doi.org/10.1038/nm.2536.

[31] T. Kelkka, et al., Mice lacking NCF1 exhibit reduced growth of implanted melanoma and carcinoma tumors, PLoS One (2013), https://doi.org/10.1371/journal.pone.0084148.

[32] M.H. Yoo, X.M. Xu, B.A. Carlson, V.N. Gladyshev, D.L. Hatfield, Thioredoxin reductase 1 deficiency reverses tumor phenotype and tumorigenicity of lung carcinoma cells, J. Biol. Chem. (2006), https://doi.org/10.1074/jbc.C600012200.

[33] T. Zou, et al., A binuclear gold(I) complex with mixed bridging diphosphine and bis (N-heterocyclic carbene) ligands shows favorable thiol reactivity and inhibits tumor growth and angiogenesis in vivo, Angew. Chem. Int. Ed. (2014), https://doi.org/10.1002/anie.201400142.

[34] K. Anestål, S. Prast-Nielsen, N. Cenas, E.S.J. Arnér, Cell death by SecTRAPs: thioredoxin reductase as a prooxidant killer of cells, PLoS One (2008), https://doi.org/10.1371/journal.pone.0001846.

[35] W. Hu, Q. Lu, Impact of oxidative stress on the cytoskeleton of pancreatic epithelial cells, Exp. Ther. Med. 8 (2014) 1438–1442.

[36] A. Sinha, T.T.T. Chu, M. Dao, R. Chandramohanadas, Single-cell evaluation of red blood cell bio-mechanical and nano-structural alterations upon chemically induced oxidative stress, Sci. Rep. 51 (5) (2015) 1–8, 2015.

[37] M.H. Antonelou, et al., Oxidative stress-associated shape transformation and membrane proteome remodeling in erythrocytes of end stage renal disease patients on hemodialysis, J. Proteomics 74 (2011) 2441–2452.

[38] A.E. Damdimopoulos, A. Miranda-Vizuete, E. Treuter, J.Å. Gustafsson, G. Spyrou, An alternative splicing variant of the selenoprotein thioredoxin reductase is a modulator of estrogen signaling, J. Biol. Chem. (2004), https://doi.org/10.1074/jbc.M402753200.

[39] I. Nalvarte, A.E. Damdimopoulos, J. Rüegg, G. Spyrou, The expression and activity of thioredoxin reductase 1 splice variants v1 and v2 regulate the expression of genes associated with differentiation and adhesion, Biosci. Rep. (2015), https://doi.org/10.1042/BSR20150236.

[40] A.K. Rundlöf, M. Janard, A. Miranda-Vizuete, E.S.J. Arner, Evidence for intriguingly complex transcription of human thioredoxin reductase 1, Free Radic. Biol. Med. (2004), https://doi.org/10.1016/j.freeradbiomed.2003.12.004.

[41] Q.A. Sun, et al., Heterogeneity within animal thioredoxin reductases. Evidence for alternative first exon splicing, J. Biol. Chem. (2001), https://doi.org/10.1074/jbc.M004750200.

[42] A.A. Saei, et al., System-wide identification and prioritization of enzyme substrates by thermal analysis, Nat. Commun. 12 (2021) 1296.

[43] A.A. Saei, et al., Comparative proteomics of dying and surviving cancer cells improves the identification of drug targets and sheds light on cell life/death decisions, Mol. Cell Proteom. 17 (2018) 1144–1155.

[44] A. Atlante, et al., Cytochrome c is released from mitochondria in a reactive oxygen species (ROS)-dependent fashion and can operate as a ROS scavenger and as a respiratory substrate in cerebellar neurons undergoing excitotoxic death, J. Biol. Chem. (2000), https://doi.org/10.1074/jbc.M002361200.

[45] E. Gottlieb, S.M. Armour, M.H. Harris, C.B. Thompson, Mitochondrial membrane potential regulates matrix configuration and cytochrome c release during apoptosis, Cell Death Differ. 10 (2003) 709–717.

[46] R.P. Herzig, S. Scacco, R.C. Scarpulla, Sequential serum-dependent activation of CREB and NRF-1 leads to enhanced mitochondrial respiration through the induction of cytochrome c, J. Biol. Chem. (2000), https://doi.org/10.1074/jbc.275.17.13134.

[47] S. Talbot, R. Nelson, W.T. Self, Arsenic trioxide and auranofin inhibit selenoprotein synthesis: implications for chemotherapy for acute promyelocytic leukaemia, Br. J. Pharmacol. (2008), https://doi.org/10.1038/bjp.2008.161.

[48] S.B. Wall, et al., Auranofin-mediated NRF2 induction attenuates interleukin 1 beta expression in alveolar macrophages, Antioxidants 10 (2021).

[49] A.P. Kipp, S. Deubel, E.S.J. Arnér, K. Johansson, Time- and cell-resolved dynamics of redox-sensitive Nrf2, HIF and NF-κB activities in 3D spheroids enriched for cancer stem cells, Redox Biol. 12 (2017) 403–409.

[50] D. Malhotra, et al., Global mapping of binding sites for Nrf2 identifies novel targets in cell survival response through chip-seq profiling and network analysis, Nucleic Acids Res. (2010), https://doi.org/10.1093/nar/gkq212.

[51] A.G. Cox, K.K. Brown, E.S.J. Arner, M.B. Hampton, The thioredoxin reductase inhibitor auranofin triggers apoptosis through a Bax/Bak-dependent process that involves peroxiredoxin 3 oxidation, Biochem. Pharmacol. (2008), https://doi.org/10.1016/j.bcp.2008.08.021.

[52] A.Y. Shih, et al., Induction of the Nrf2-driven antioxidant response confers neuroprotection during mitochondrial stress in vivo, J. Biol. Chem. (2005), https://doi.org/10.1074/jbc.M414635200.

[53] K.M. Holmström, R.V. Kostov, A.T. Dinkova-Kostova, The multifaceted role of Nrf2 in mitochondrial function, Curr. Opin. Toxicol. (2016), https://doi.org/10.1016/j.cotox.2016.10.002.

[54] Q. Li, et al., Thioredoxin reductase inhibition attenuates neonatal hyperoxic lung injury and enhances nuclear factor E2-related factor 2 activation, Am. J. Respir. Cell Mol. Biol. 55 (2016) 419–428.

[55] Y. Fuse, et al., The possible repositioning of an oral anti-arthritic drug, auranofin, for Nrf2-activating therapy: The demonstration of Nrf2-dependent anti-oxidative action using a zebrafish model, 115, 2018, pp. 405–411.

[56] M. Cebula, E.E. Schmidt, E.S.J. Arnér, TrxR1 as a potent regulator of the Nrf2-Keap1 response system, Antioxidants Redox Signal. (2015), https://doi.org/10.1089/ars.2015.6378.

[57] Q. Cheng, T. Sandalova, Y. Lindqvist, E.S.J. Arnér, Crystal structure and catalysis of the selenoprotein thioredoxin reductase 1, J. Biol. Chem. (2009), https://doi.org/10.1074/jbc.M807068200.

[58] Q. Cheng, et al., The selenium-independent inherent pro-oxidant NADPH oxidase activity of mammalian thioredoxin reductase and its selenium-dependent direct peroxidase activities, J. Biol. Chem. (2010), https://doi.org/10.1074/jbc.M110.117259.

[59] V. Mostert, K.E. Hill, R.F. Burk, Loss of activity of the selenoenzyme thioredoxin reductase causes induction of hepatic heme oxygenase-1, FEBS Lett. (2003), https://doi.org/10.1016/S0014-5793(03)00309–0.

[60] M. Martin, R.E. Rehani, R.S. Jope, S.M. Michalek, Toll-like receptor - mediated cytokine production is differentially regulated by glycogen synthase kinase 3, Nat. Immunol. (2005), https://doi.org/10.1038/ni1221.

[61] R.S. Schrecengost, et al., In vitro and in vivo antitumor and anti-inflammatory capabilities of the novel GSK3 and CDK9 inhibitor ABC183s, J. Pharmacol. Exp. Therapeut. (2018), https://doi.org/10.1124/jpet.117.245738.

[62] H. Sedlackova, et al., Equilibrium between nascent and parental MCM proteins protects replicating genomes, Nature (2020), https://doi.org/10.1038/s41586-020-2842-3.

[63] A. Nishiyama, L. Frappier, M. Méchali, MCM-BP regulates unloading of the MCM2-7 helicase in late S phase, Genes Dev. (2011), https://doi.org/10.1101/gad.614411.

[64] C.S.H. Tan, et al., Thermal proximity coaggregation for system-wide profiling of protein complex dynamics in cells, Science (80-.). 359 (2018) 1170–1177.

[65] L.F. Boullosa, et al., Auranofin reveals therapeutic anticancer potential by triggering distinct molecular cell death mechanisms and innate immunity in mutant p53 non-small cell lung cancer, Redox Biol. (2021) 101949, https://doi.org/10.1016/j.redox.2021.101949.

[66] M. Quimbaya, et al., Deregulation of the replisome factor MCMBP prompts oncogenesis in colorectal carcinomas through chromosomal instability, Neoplasia (2014), https://doi.org/10.1016/j.neo.2014.07.011.

[67] M. Simonović, A.K. Puppala, On elongation factor eEFSec, its role and mechanism during selenium incorporation into nascent selenoproteins, Biochim. Biophys. Acta Gen. Subj. 1862 (2018) 2463–2472.

[68] C. Tang, et al., Selenium deficiency-induced redox imbalance leads to metabolic reprogramming and inflammation in the liver, Redox Biol. (2020), https://doi.org/10.1016/j.redox.2020.101519.

[69] X. Huang, et al., Selenium deficiency induced injury in chicken muscular stomach by downregulating selenoproteins, Biol. Trace Elem. Res. (2017), https://doi.org/10.1007/s12011-017-0946-x.

[70] P.A. Khoso, Z. Yang, C. Liu, S. Li, Selenium deficiency downregulates selenoproteins and suppresses immune function in chicken thymus, Biol. Trace Elem. Res. (2015), https://doi.org/10.1007/s12011-015-0282-y.

[71] F. Radenkovic, O. Holland, J.J. Vanderlelie, A.V. Perkins, Selective inhibition of endogenous antioxidants with Auranofin causes mitochondrial oxidative stress which can be countered by selenium supplementation, Biochem. Pharmacol. (2017), https://doi.org/10.1016/j.bcp.2017.09.009.

[72] K.C. Chang, J.M. Petrash, Aldo-keto reductases: multifunctional proteins as therapeutic targets in diabetes and inflammatory disease, in: Adv. Exp. Med. Biol., 2018, https://doi.org/10.1007/978-3-319-98788-0_13.

[73] T.M. Penning, The aldo-keto reductases (AKRs): Overview, Chem. Biol. Interact. (2015), https://doi.org/10.1016/j.cbi.2014.09.024.

[74] M. Gagliardi, et al., Aldo-keto reductases protect metastatic melanoma from ER stress-independent ferroptosis, Cell Death Dis. (2019), https://doi.org/10.1038/s41419-019-2143-7.

[75] T. Matsunaga, et al., Pathophysiological roles of autophagy and aldo-keto reductases in development of doxorubicin resistance in gastrointestinal cancer cells, Chem. Biol. Interact. (2019), https://doi.org/10.1016/j.cbi.2019.108839.

[76] R. Yan, et al., Aldo-keto reductase family 1 B10 gene silencing results in growth inhibition of colorectal cancer cells: implication for cancer intervention, Int. J. Cancer (2007), https://doi.org/10.1002/ijc.22933.

[77] C. Gao, et al., Aldo-keto reductase family 1 member B induces aortic valve calcification by activating hippo signaling in valvular interstitial cells, J. Mol. Cell. Cardiol. (2021), https://doi.org/10.1016/j.yjmcc.2020.10.002.

[78] S. Endo, et al., Synthesis of potent and selective inhibitors of aldo-keto reductase 1B10 and their efficacy against proliferation, metastasis, and cisplatin resistance of lung cancer cells, J. Med. Chem. (2017), https://doi.org/10.1021/acs.jmedchem.7b00830.

[79] R. Khayami, S.R. Hashemi, M.A. Kerachian, Role of aldo-keto reductase family 1 member B1 (AKR1B1) in the cancer process and its therapeutic potential, J. Cell Mol. Med. (2020), https://doi.org/10.1111/jcmm.15581.

[80] T.M. Penning, J.E. Drury, Human aldo-keto reductases: function, gene regulation, and single nucleotide polymorphisms, Arch. Biochem. Biophys. 464 (2007) 241–250.

[81] Q. Cheng, E.S.J. Arnér, Overexpression of recombinant selenoproteins in E. coli, in: Methods Mol. Biol. 1661, 2018, pp. 231–240 (Humana Press, New York, NY).